Since January 2020 Elsevier has created a COVID-19 resource centre with free information in English and Mandarin on the novel coronavirus COVID-19. The COVID-19 resource centre is hosted on Elsevier Connect, the company's public news and information website.

Antiviral Research 173 (2020) 104651

Contents lists available at ScienceDirect

Antiviral Research

journal homepage: www.elsevier.com/locate/antiviral

Receptor tyrosine kinase inhibitors block proliferation of TGEV mainly through p38 mitogen-activated protein kinase pathways

Wanyu Dong[a,b,c,d], Wenting Xie[a,b], Yunbo Liu[a,b], Baokun Sui[a,b], Hao Zhang[a,b], Liran Liu[a,b], Yubei Tan[a,b], Xiaohan Tong[a,b], Zhen F. Fu[a,b,e], Ping Yin[c], Liurong Fang[a,b], Guiqing Peng[a,b,*]

[a] The State Key Laboratory of Agricultural Microbiology, College of Veterinary Medicine, Huazhong Agricultural University, Wuhan, 430070, China
[b] The Cooperative Innovation Center for Sustainable Pig Production, Huazhong Agricultural University, Wuhan, 430070, China
[c] National Key Laboratory of Crop Genetic Improvement, National Centre of Plant Gene Research, College of Life Science and Technology, Huazhong Agricultural University, Wuhan, 430070, China
[d] Department of Veterinary Medicine, College of Animal Science and Technology, Zhejiang A&F University, Hangzhou, 311300, China
[e] Departments of Pathology, College of Veterinary Medicine, University of Georgia, Athens, GA, 30602, USA

ARTICLE INFO

Keywords:
Receptor tyrosine kinase inhibitor
Virus-host interaction
Comparative phosphoproteomic
Anti-coronaviral therapy

ABSTRACT

Emerging coronaviruses (CoVs) primarily cause severe gastroenteric or respiratory diseases in humans and animals, and no approved therapeutics are currently available. Here, A9, a receptor tyrosine kinase inhibitor (RTKI) of the tyrphostin class, is identified as a robust inhibitor of transmissible gastroenteritis virus (TGEV) infection in cell-based assays. Moreover, A9 exhibited potent antiviral activity against the replication of various CoVs, including murine hepatitis virus (MHV), porcine epidemic diarrhea virus (PEDV) and feline infectious peritonitis virus (FIPV). We further performed a comparative phosphoproteomic analysis to investigate the mechanism of action of A9 against TGEV infection in vitro. We specifically identified p38 and JNK1, which are the downstream molecules of receptor tyrosine kinases (RTKs) required for efficient TGEV replication, as A9 targets through plaque assays, qRT-PCR and Western blotting assays. p38 and JNK1 inhibitors and RNA interference further showed that the inhibitory activity of A9 against TGEV infection was mainly mediated by the p38 mitogen-activated protein kinase (MAPK) signaling pathway. All these findings indicated that the RTKI A9 directly inhibits TGEV replication and that its inhibitory activity against TGEV replication mainly occurs by targeting p38, which provides vital clues to the design of novel drugs against CoVs.

1. Introduction

Coronaviruses (CoVs) are enveloped viruses possessing a single-stranded, positive-sense RNA genome and belong to the family Coronaviridae and the order Nidovirales. The CoV genome is currently the largest known viral RNA genome, with a total length of 28–30 kb. CoVs consist of four genera: *Alpha-*, *Beta-*, *Gamma-*, and a tentative new genus, *Deltacoronavirus* (de Groot et al., 2012). CoVs commonly cause gastroenteric or respiratory diseases in animal hosts as well as in humans. Given that there are currently no approved vaccines or antiviral strategies for many pathogenic CoVs (Ramajayam et al., 2010), it is increasingly important to identify broad-spectrum antiviral compounds. These compounds will promote quick responses to threats of new or changing pandemics, possibly even without accurate identification of the agents.

Transmissible gastroenteritis virus (TGEV), the causative agent of porcine transmissible gastroenteritis, together with porcine epidemic diarrhea virus (PEDV), human CoVs 229E (HCoV-229E) and canine CoVs (CCoVs), belong to *Alpha coronavirus* (Carstens, 2010). TGEV causes fatal acute diarrhea, vomiting, and dehydration, with mortality rates of nearly 100% in suckling piglets less than 2 weeks old (Pritchard et al., 1999), resulting in severe economic losses in the swine industry worldwide. Approximately two-thirds of the 5′-proximal region of the TGEV genome encodes the replicase gene (rep), which contains two open reading frames (ORF1a and ORF1b). Polyprotein 1a (pp1a) and polyprotein 1 ab (pp1ab) are translated by rep (Gorbalenya et al., 2006) and are proteolytically processed by virus-encoded proteases into 16 non-structural proteins (nsps), nsps 1–16, many of which have enzymatic activities, such as papain-like protease (PLP or nsp3), 3C-like protease (3CL), RNA-dependent RNA polymerase (RdRp, nsp12), and

* Corresponding author. State-key Laboratory of Agricultural Microbiology, College of Veterinary Medicine, Huazhong Agricultural University, Wuhan, 430070, China.
E-mail address: penggq@mail.hzau.edu.cn (G. Peng).

https://doi.org/10.1016/j.antiviral.2019.104651
Received 26 April 2019; Received in revised form 13 November 2019; Accepted 16 November 2019
Available online 18 November 2019
0166-3542/

helicase (nsp13). These nsps along with putative cellular factors are believed to form replication/transcription complexes, which play an important role in CoV RNA transcription and replication (Neuman et al., 2014). As the crystal structures of a large number of viral non-structural and structural proteins have been solved, targeted drug design has been attempted (Tong, 2009). Unfortunately, such efforts have not led to advances in antiviral drugs beyond the preclinical stage (Hilgenfeld and Peiris, 2013). Overall, this target-based approach ignores other possible targets, including host cell signaling pathways or other host factors that are essential for CoV replication. Furthermore, RNA viral genomes typically replicate with low fidelity and undergo rapid evolutionary changes. Thus, targeting cellular factors involved in virus infection provides an excellent strategy for drug development because such treatment is not easily evaded by the high mutation rates in viral genomes (Zhou et al., 2011).

Protein kinases and phosphatases involve a wide variety of cellular functions. Receptor tyrosine kinases (RTKs) are a group of growth factor receptors and key components of the biological control networks that regulate many biological processes including cell proliferation and differentiation as well as survival (Lemmon and Schlessinger, 2010). RTKs also play an important role in transforming extracellular and intracellular signals and activating or linking them to downstream signaling pathways, such as the Ras/mitogen-activated protein kinase (MAPK), PI3K/Akt, and JAK/STAT pathways (Pawson, 1995; Schlessinger, 2000). As RTKs are both master regulators of normal cellular processes and play a vital role in the development and progression of various cancers, they have been extensively studied as targets for the treatment of many types of malignancies (Roussidis and Karamanos, 2002). Recently, a growing number of studies has shown that several RTKs and other tyrosine kinases are involved in viral replication. For example, the receptor tyrosine kinase AXL can function as an entry factor for dengue virus and Zika virus (ZIKV) (Meertens et al., 2012; Meertens et al., 2017). In addition, the protein tyrosine kinase inhibitor genistein was shown to block the replication of type-1 human immunodeficiency virus (HIV-1), herpes simplex virus type 1 (HSV-1), and arenaviruses (Stantchev et al., 2007; Vela et al., 2008; Yura et al., 1993). PTP1B, the protein tyrosine phosphatase was also shown to be a target for antiviral therapy (Carbone et al., 2012). Imatinib, an Abelson (Abl) kinase inhibitor, was shown to be a potent inhibitor of both SARS-CoV and MERS-CoV in vitro (Dyall et al., 2014). Two RTK inhibitors (RTKIs), known as AG879 and tyrphostin A9, can block multiple steps of influenza A virus replication, but both the underlying mechanism of this inhibitory effect and its target are unclear (Kumar et al., 2011a; Kumar et al., 2011b). The Raf/MEK/ERK pathways downstream of RTKs are involved in murine hepatitis virus (MHV) RNA synthesis (Cai et al., 2007), and a recent study indicated that epidermal growth factor receptor (EGFR) is a promoter for TGEV entry (Hu et al., 2016).

In the current study, we used the model *alpha-coronavirus* TGEV to screen inhibitors of CoV replication using a high-throughput assay based on the pronounced cytopathic effect (CPE) caused by TGEV infection in PK-15 cells. We identified tyrphostin A9 (A9), a specific RTKI, as having a strong antiviral activity against TGEV. In addition, A9 appears to be a broad-spectrum CoV inhibitor, as it blocked the replication of MHV, PEDV and feline infectious peritonitis virus (FIPV) with comparable efficacy. Furthermore, we employed both pharmacological inhibitors and RNA interference to demonstrate that A9 dramatically suppresses viral replication and viral RNA synthesis mainly through the p38 signaling pathway. Our findings provide molecular insight into the potential role of host RTK signaling pathways in promoting the replication of CoVs and suggest that tyrphostin A9 could be developed as a potential anti-CoV therapy.

2. Materials and methods

2.1. Cell lines, viruses and reagents

PK-15, ST, Vero-CCL81 (African green monkey kidney epithelial cells) and CCL94 (Cat kidney epithelial cells) were maintained at 37 °C with a 5% CO_2 incubator in Dulbecco's modified Eagle's medium (DMEM, Invitrogen, Carlsbad, CA, USA) supplemented with 10% fetal bovine serum (FBS) and penicillin-streptomycin (50 units/ml). FIPV 79–1146 was purchased from American Type Culture Collection (ATCC®; Manassas, VA, USA). The PEDV YN144 strain (GenBank accession number: **KT021232.1**) and TGEV WH-1 strain (GenBank accession number: **HQ462571.1**) were isolated from suckling piglets. PEDV and FIPV were propagated in Vero-CCL81 and CCL94 cells, respectively. TGEV was grown in PK-15 or ST cells. The viral titers were determined by plaque assay on PK-15 (TGEV), Vero-CCL81 (PEDV) or CCL94 (FIPV) cells. Infection of cultured cells with PEDV was conducted in the presence of trypsin at a concentration of 5 μg/ml with serum-free medium.

Library of Pharmacologically Active Compounds 1280 (LOPAC^{1280}) was purchased from Sigma-Aldrich, each compound was dissolved to 10 mM in dimethyl sulfoxide (DMSO) and stored at −20 °C. Tyrphostin A9, ribavirin and flunarizine were purchased from Sigma. The p38 inhibitor BIRB796 and the JNK1 inhibitor DB07268 were obtained from ApexBio. LY222820 was purchased from TargetMol. A GAPDH-specific monoclonal antibody was purchased from Proteintech (Chicago, IL, USA). Antibodies against p38, Jun-N-terminal kinases (JNKs), phosphorylated p38 (p-p38) and phosphorylated JNKs (p-JNKs) were purchased from Cell Signaling Technology (Washington, DC, USA). The anti-phosphorylated p38 (p-p38) antibody is specific for Y182 and T180. The anti-TGEV N polyclonal antibody was prepared in our laboratory.

2.2. Cell viability assay

Tyrphostin A9, BIRB796 and DB07268 were stored as 50 mM stock solutions in DMSO. LY222820 was stored as a 10 mM stock solution in DMSO. The cytotoxic effect of reagents on cell viability was measured in 96-well plates using CellTiter-Glo (Promega) according to the manufacturer's protocol. Cell viability was determined using a Veritas microplate luminometer (Promega) with values normalized to those of untreated cells. Accordingly, throughout this work, no cytotoxicity was observed for A9 at 6 μM, BIRB796 at 80 μM, DB07268 at 35 μM or LY222820 at 45 μM.

2.3. Antiviral assays

The effects of A9 on the infection of TGEV in PK-15 or ST cells, PEDV in Vero cells, FIPV in CCL-94 cells, and MHV in L929 cells were determined by comparing the levels of viral replication in target cells in the absence or presence of A9. Target cells were pretreated in triplicate with DMSO or A9 (4 μM) for 1 h, followed by virus infection at a multiplicity of infection (MOI) of 0.1. Cell supernatants were harvested at 16–24 h post infection (hpi), and viral titers were quantified by plaque formation assays.

To assess the effect of the inhibitors of JNK and P38 on TGEV, PK-15 cells were infected with TGEV and treated with BIRB796, DB07268 or DMSO. The culture supernatants were collected at different time points (6, 12, 24, 36, and 48 hpi) and stored at −80 °C. The TGEV titer was determined by plaque assay using PK-15 cells as described previously (Zhang et al., 2012) and quantified as plaque-forming units (PFUs) per ml.

2.4. Time-of-addition assay

The antiviral mechanism of A9 was determined by time-of-addition assay as previously described (Basu et al., 2011); the procedure is shown schematically in Fig. 2A. PK-15 cells were infected with TGEV at an MOI of 0.1 for 1 h (0 h). A9 at 4 μM was added to the cells at 1 h pre-infection (−1 h), during infection (0 h), and 1 h post-infection (+1 h). To exclude a possible direct inactivating effect of A9 on TGEV, the virus

was incubated with A9 at 4 °C for 1 h, and the mixtures were used to infect PK-15 cells for 1 h. Duplicate wells were used for each process. Cell cultures treated with the drug vehicle (DMSO) were used as a control. At 24 hpi, the culture medium was harvested for virus titration.

2.5. Virus inoculation and sample preparation

The samples used for quantitative proteomic analysis consisted of four groups: PK-15 cells infected at an MOI of 1 with TGEV, uninfected cells that were treated with A9, uninfected cells that were treated with DMSO, and PK-15 cells infected with TGEV and treated with A9. At 24 hpi, the cells were collected for protein extraction, digestion, and labeling.

2.6. Protein isolation and labeling with tandem mass tags

Cell samples from four groups were collected with cell scrapers and washed twice with ice-cold phosphate-buffered saline (PBS) containing the protease inhibitor cocktail. The cells were lysed in 500 μL of lysis buffer, and the remaining debris was removed by centrifugation at 12,000 × *g* at 4 °C for 10 min. The supernatant was collected and the protein concentration was determined with a bicinchoninic acid (BCA) kit according to the manufacturer's instructions. Trypsin was added to the protein solution at a 1:50 trypsin-to-protein mass ratio for a first digestion overnight and at a 1:100 trypsin-to-protein mass ratio for a second 4 h-digestion. The peptides were then labeled with different TMT tags and the labeled samples were mixed, desalted and dried by vacuum centrifugation.

2.7. LC-MS/MS analysis

After fractionation by high-pH reverse-phase HPLC using a Thermo Betasil C18 column, the tryptic peptides were dissolved in 0.1% formic acid (solvent A) and directly loaded onto a homemade reverse-phase analytical column (15-cm length, 75 μm i.d.). The gradient comprised an increase from 6% to 23% solvent B (0.1% formic acid in 98% acetonitrile) over 26 min, a further increase from 23% to 35% over 8 min and a climb to 80% in 3 min; the concentration was held at 80% for the last 3 min. All steps were performed at a constant flow rate of 400 nL/min with an EASY-nLC 1000 ultra-performance liquid chromatography (UPLC) system. The peptides were subjected to a nanoelectrospray ionization (NSI) source followed by tandem mass spectrometry (MS/MS) with a Q Exactive™ Plus instrument (Thermo) that was coupled online to the UPLC. The applied electrospray voltage was 2.0 kV. The m/z scan range was 350 to 1800 for full scans, and intact peptides were detected in the Orbitrap at a resolution of 70,000. Peptides were then selected for MS/MS using a normalized collision energy (NCE) setting of 28, and the fragments were detected in the Orbitrap at a resolution of 17,500. A data-dependent procedure that alternated between one MS scan and 20 MS/MS scans with 15.0 s of dynamic exclusion was used. The automatic gain control (AGC) was set at 5E4. The fixed first mass was set as 100 m/z.

2.8. Quantitative real-time RT-PCR

PK-15 cells were treated with BIRB796, DB07268 or DMSO for 2 h prior to infection with TGEV at 0.1 MOI for 1 h at 37 °C. Total RNA from PK-15 cells was extracted using TRIzol Reagent (Invitrogen, Grand Island, NY) after 6, 12, 18, 24 or 36 hpi, respectively. cDNA was generated using the ReverTra Ace qPCR RT Kit (Toyobo, Japan) according to the manufacturer's instructions. Quantitative real-time PCR was performed using SYBR green (Bio-Rad). N gene expression was calculated using a relative quantification ($2^{-\Delta\Delta CT}$) model and normalized to that of the internal control GAPDH. The primers targeting the TGEV N protein and GAPDH were as follows: TGEV N-specific primers (forward, 5′-GAGCAGTGCCAAGCATTACCC-3'; reverse, 5′-GACTTCTAT CTGGTC GCCATCTTC-3′) GAPDH-specific primers (forward, 5′-ACATGGCCTCC AAGGAGTAAGA-3'; reverse, 5′-GATCGAGTTGGGGCTGTGACT-3′).

2.9. RNA interference

Specific pig p38 siRNA sequences were obtained from a published paper (Gan et al., 2017) and synthesized by Genepharma (Shanghai, China). NC siRNA was purchased from Genepharma. The sequence of the p38-specific siRNA sequence was 5′-GCAGGAGCUGAACAAGACAtt-3'. siRNA transfection was performed with transfection reagent according to the manufacturer's instructions, and the efficiency of the siRNA was characterized by Western blotting. The proportion of the target protein was calculated using ImageJ software. PK-15 cells were transfected with p38 siRNA or NC siRNA; after 48 h, the cells were infected with 0.1 MOI TGEV and treated with A9 for 12 h or infected with 0.1 MOI TGEV only. Cells treated with TGEV and DMSO at 48 h post transfection were used as controls. Virus yield in supernatants of the cultures was detected by the plaque assay.

2.10. Western blot analyses

PK-15 cells were cultured in six-well plates and were mock-infected or infected with TGEV at an MOI of 0.1. At the indicated post infection times, cells were harvested with lysis buffer (Beyotime, China) containing protease inhibitors and were boiled for 10 min with sample loading buffer (Beyotime, China). The samples were fractionated by SDS-PAGE. Gels were transferred onto polyvinylidene difluoride (PVDF) (Merck Millipore, USA), blocked in 5% bovine serum albumin or 5% dried skimmed milk in TBS (20 mM Tris-HCl [pH 7.5], 150 mM NaCl) at room temperature for 2 h and then incubated with the indicated primary antibodies. After washing three times, the membranes were exposed to a species-specific horseradish peroxidase-conjugated secondary antibody for another 1 h and washed three times followed by enhanced chemiluminescence (ECL, Thermo Scientific) detection by autoradiography (Bio-Rad). GAPDH was used as a loading control.

2.11. Statistical analysis

All experiments were performed in triplicate. Data are presented as the mean ± standard deviation (SD). The differences in means were analyzed by Student's *t*-test. P values less than 0.05 were considered statistically significant (*$p < 0.05$, **$p < 0.01$, and ***$p < 0.001$).

3. Results

3.1. Identification of TGEV inhibitors by high-throughput screening of a compound library

To achieve a robust signal for high-throughput screening (HTS), the PK-15 cell number, MOI, and assay endpoint were optimized to meet the conditions of S/B > 5, Z′ > 0.5 and CV < 10%. We then screened the Library of Pharmacologically Active Compounds 1280 for anti-TGEV activity under the optimized conditions using a CPE-based HTS assay. Two compounds, flunarizine and A9, exerted strong inhibitory effects on TGEV replication in vitro and their structures are shown in Fig. 1A.

To eliminate cytotoxic effects, cell viability at various concentrations of flunarizine or A9 was evaluated using the MTT assay (Fig. 1B and D). Ribavirin has previously been reported to inhibit MERS-CoV replication (Falzarano et al., 2013) and was thus used as a positive control. Compared to the DMSO control, flunarizine and ribavirin were not cytotoxic in PK-15 cells at concentrations up to 10 μM and 90 μM, respectively (Fig. 1B). Subsequent MTT assays showed no cytotoxicity up to 6 μM A9 (Fig. 1D). To compare antiviral potencies, PK-15 cells were infected with TGEV at an MOI of 0.1 and then treated with DMSO or compounds at various concentrations, and the virus yield in the

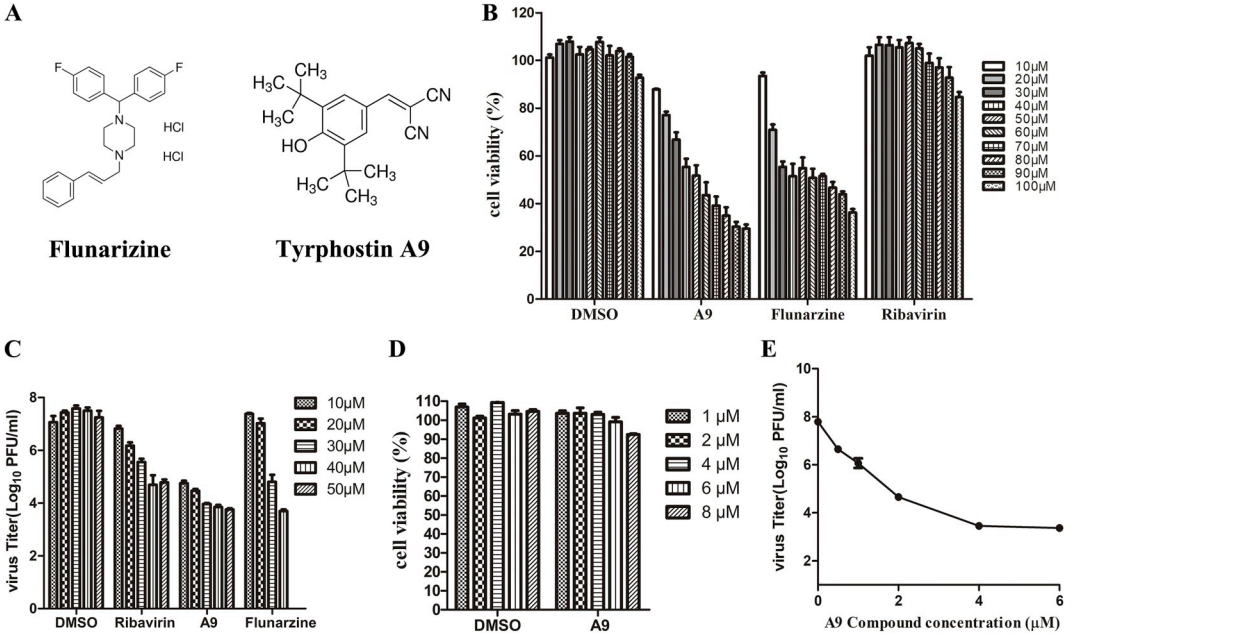

Fig. 1. Characterization of the identified compounds with regard to cytotoxicity and anti-TGEV efficacy. (A) Chemical structures of flunarizine and tyrphostin A9. (B) and (D) Determination of cytotoxicity of the compounds in PK-15 cells by the MTT assay. PK-15 cells were incubated with various concentrations of the compounds or the vehicle control DMSO for 48 h and cell viability was measured by MTT assay. (C) and (E) Dose-dependent inhibition of TGEV in PK-15 cells by the different compounds. PK-15 cells were infected with TGEV at an MOI of 0.1 in the presence of various concentrations of the compounds or vehicle control DMSO. Viral yields at 24 hpi were detected by plaque assay. The results shown in panels B to E are the means of at least three independent experiments.

supernatants was determined at 36 hpi (Fig. 1C and E). Compared to the vehicle control (DMSO), both A9 and ribavirin displayed dose-dependent inhibitory activities against TGEV in PK-15 cells. No inhibition was observed by treating cells with 10 μM flunarizine, a concentration that was not cytotoxic. Note that the strong viral inhibition produced by flunarizine at 30 μM and A9 at 10 μM might be due to cytotoxicity at those concentrations (Fig. 1C). Based on the cytotoxicity and antiviral efficacy results, we chose A9 at 4 μM for further evaluation in this study. Taken together, these initial studies identified A9 as a specific RTKI that can strongly suppress the TGEV yield.

3.2. The inhibitory effect of A9 on TGEV production is neither cell type specific nor virus-to-cell ratio specific

To explore whether the antiviral activity of A9 is affected by the cell type or virus-to-cell ratio, viral inhibition assays were performed in epithelial and fibroblast derived cell types and at various MOIs. Both PK-15 and ST cells were treated with A9 or vehicle control (DMSO) and infected with TGEV at an MOI of 0.01, 0.1, or 1. As peaks of TGEV replication at different MOIs were observed at various time points, the viral yield in the supernatants was quantified at 48 h (MOI = 0.01), 24 h (MOI = 0.1), or 12 h (MOI = 1) post infection. As shown in Fig. 2A and B, A9 strongly inhibited TGEV production in the two cell lines and at all tested virus-to-cell ratios, although some variation between the cell types was observed. In addition, a 1 to > 4 log decrease in infectious progeny was observed in the A9 treatment group compared to that of the DMSO treatment control. Taken together, the results demonstrate that the inhibition of TGEV replication by A9 is not limited to a single cell type and is effective even with relatively high levels of input virus. Compared with its behavior in ST cells, A9 displayed greater inhibition against TGEV in PK-15 cells. One explanation for this difference may be that A9 uptake differs per cell line.

3.3. A9 mainly acts at the post-adsorption stage of the TGEV life cycle

To determine the specific step(s) of the TGEV life cycle inhibited by A9, we performed time-of-addition assays. PK-15 cells were treated with A9 1 h before TGEV infection (−1 h), at the same time as infection (0 h) and 1 h post-TGEV infection (1 h) (Fig. 2C). TGEV infected PK-15 cells were treated with DMSO as a control. The titer of infectious viral particles in the supernatant at 24 hpi was measured by plaque assays. When added at either 4 °C or 37 °C during (0 h) virus infection, A9 displayed relatively slight inhibitory activity against the TGEV infection (Fig. 2D), suggesting that A9 has a low effect on virus binding and entry. In addition, there was no significant decrease in virus yield compared to the DMSO-treated control when A9 was added before TGEV attachment. Interestingly, when A9 was added 1 h post TGEV infection, the virus yields were reduced by more than 3 logs. These findings indicated that A9 mainly blocks the post-adsorption stage of the TGEV life cycle. Additionally, the inhibitory effect of A9 is likely exerted through cellular mechanisms rather than directly by reducing virion infectivity.

3.4. A9 exhibits broad-spectrum anti-CoV activity

To investigate whether the TGEV inhibitor A9 is a potential broad-spectrum CoV inhibitor, we assessed its activity against three additional CoVs: the *betacoronavirus* MHV (strain A59) and the *alphacoronaviruses* FIPV and PEDV. The initial cell viability assay verified that A9 did not result in any signs of toxicity in Vero-CCL81, CCL-94 and A549 cells at concentrations up to 4 μM (data not shown). Cells were treated with A9 at 4 μM or with DMSO, followed by infection with virus at an MOI of 0.1. Cell supernatants were harvested at 16 hpi for MHV on A549 cells, 24 hpi for FIPV on CCL-94 cells or 18 hpi for PEDV on Vero-CCL81 cells and titrated by the plaque assay (Fig. 3). When an A9 dose of 4 μM was used, PEDV progeny titers were decreased by ~3 log. FIPV and MHV production were reduced by a similar extent (~4 and ~3-log reduction, respectively). The overall results demonstrate that A9 displays CoV inhibitory activity, inhibiting infectious PEDV, MHV and FIPV with similar potencies.

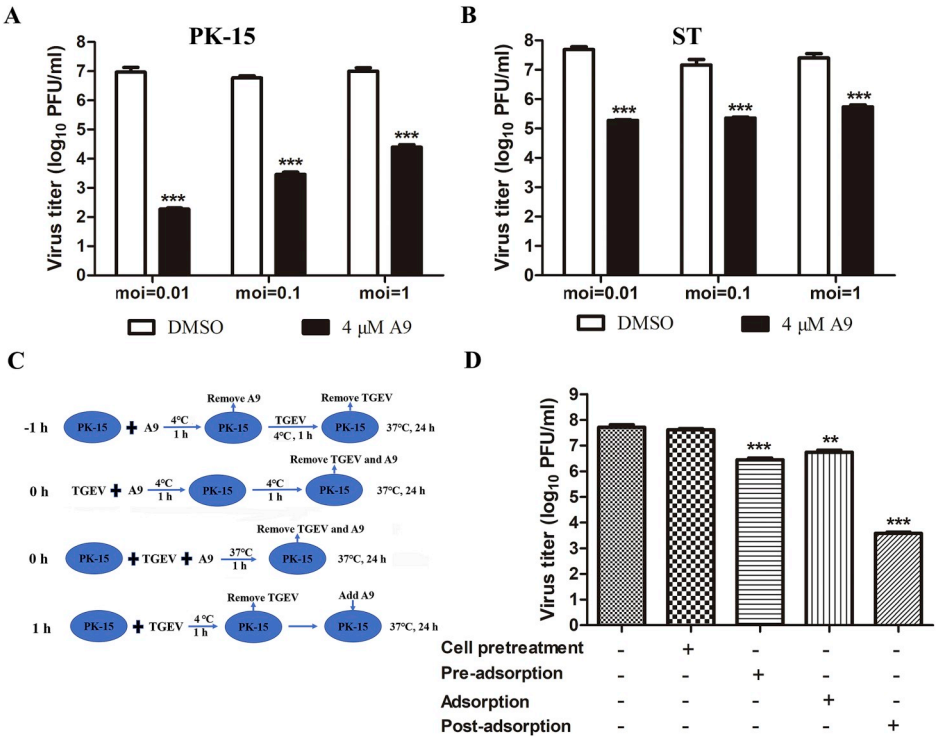

Fig. 2. A9 effectively blocks TGEV replication in cell culture. A9 blocked the multiplication of TGEV at different virus-to-cell molar ratios in both PK-15 cells (A) and ST cells (B). Viral yield in the supernatants was analyzed at 48 h (for an MOI of 0.01), 24 h (for an MOI of 0.1), or 12 h (for an MOI of 1) after infection. (C) Schematic diagram of a "time-of-addition experiment" with TGEV to determine the effect of A9 on the TGEV life cycle. (D) A9 mainly acts at the post-adsorption stage of the TGEV life cycle. PK-15 cells were infected with TGEV at an MOI of 0.1. A9 was added for 1 h before infection (−1 h), for 1 h during adsorption (0 h), and for 1 h after infection (+1 h). The virus titer at 24 hpi was determined by plaque assay. The data represent averages from at least three independent experiments, with error bars indicating standard deviations. Statistical analysis was performed using Student's *t*-test (**, $p < 0.01$; ***, $p < 0.001$).

3.5. Identification of treatment-induced changes in the cell phosphoproteome

To explore the downstream mechanism by which A9 might regulate a cellular anti-coronaviral response, we performed a comparative proteomics analysis to identify changes in the phosphorylation status using a TMT-labeled quantitative LC-MS/MS approach. PK-15 cells were subjected to four different experiments: mock control (untreated), A9 treated, TGEV-infected PK-15 cells (TGEV-infected), and TGEV infection with A9 treatment (TGEV/A9). After the three biological replicates were combined, a total of 868 phosphosites corresponding to 569 phosphorylated proteins were identified in the phosphoproteomic analysis among all groups (n = 3 for each group), of which 444 phosphorylated proteins were quantified (Table S1). The proteins that met the criteria of a $p < 0.05$ and fold-change ratios ≥ 1.5 or ≤ 0.667 were considered differentially regulated phosphoproteins (DRPs). Of the 444 phosphoproteins, 12 phosphoproteins were significantly upregulated and 5 were downregulated in the TGEV-infected group relative to those in the untreated control (Fig. S1A and Table S2). Among the 12 proteins with a > 1.5-fold increase over the proteome background, 55.55% are nuclear-encoded mitochondrial proteins (Fig. S1B and Table S3). Moreover, the levels of phosphorylated MAPK14/p38 and MAPK8/JNK1 were significantly upregulated (by > 10-fold and by > 3-fold, respectively) without any change in overall protein expression in TGEV infected samples compared with that in the mock control (Fig. S1B and Table S3). In contrast, A9 treatment reduced p38 and JNK1 phosphorylation in TGEV-infected PK-15 cells (Fig. S1 C and Table S3). Treatment with A9 alone did not affect the overall expression or phosphorylation status of p38 and JNK1 relative to the untreated control (Table S2). Surprisingly, comparison of the A9-treated group and mock control group showed that the phosphorylation statuses of multiple proteins markedly increased with A9 treatment, including elongation factor Tu (TUFM), 28S ribosomal protein S7 (MRPS7), LETM1, EF-hand domain-containing protein 1 and Delta-like protein (JAG1). In addition, the phospho-signaling of fourteen proteins decreased significantly in the A9-treated PK-15 cells compared with that in the untreated control cells (Fig. S1A and Table S2). Overall, these results reveal a strong correlation between A9 and TGEV, JNK1 and/or p38.

3.6. Functional categories and biological interaction network of the phosphoproteins differentially regulated between the TGEV/A9 and TGEV infection groups

To gain insight into the biologically relevant functions of the changes in protein phosphorylation after TGEV infection and subsequent A9 treatment, enrichment (with ≥1.5-fold change in phosphorylation) of Gene Ontology (GO) terms and functional categories

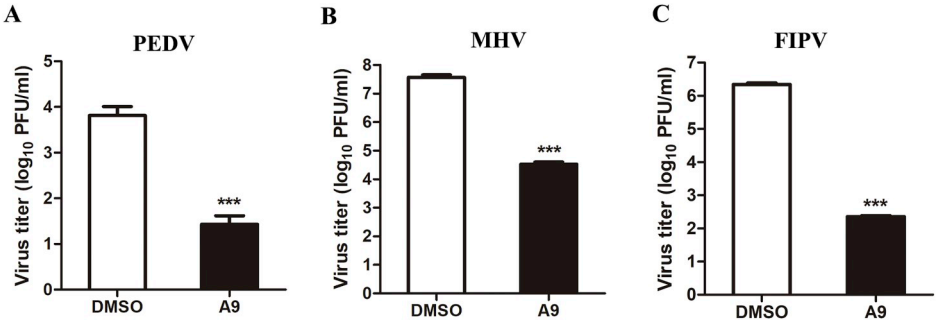

Fig. 3. A9 inhibits the replication of various coronaviruses. Inhibition PEDV(A), MHV (B) and FIPV (C) virus production at an MOI of 0.1 was achieved as described in the Materials and Methods section. Viral production was determined by plaque assay. The results shown are the means of three independent experiments. Error bars denote SD (n = 3). Statistical analysis used Student's *t*-test (***, $p < 0.001$).

was assessed. As shown in Fig. S2A and Table S4, proteins exhibiting differential phosphorylation after A9 treatment are associated with various biological processes, including cell growth, energy pathway, cell communication, protein metabolism and signal transduction. We then investigated the pathways affected by TGEV infection and subsequent A9 treatment. The results indicated that the activity of several kinase-mediated signaling pathways was increased (Fig. S2A and Table S4); these pathways included EGFR1, IL-2-mediated signaling events and MAPK pathways. We also utilized Motif-X online software (Version 1.2, http://motif-x.med.harvard.edu/) to assess the enrichment of significant motif substrates after A9 treatment, which resulted in the identification of three tyrosine-based phosphorylation motif sequences: YXXXR, KXXXXY, and YXXXXK. According to the results, the most significantly phosphorylated amino acid is tyrosine followed by threonine, YxxxRxx is also the most significant kinase motif, which is consistent with the properties of A9 as an inhibitor of RTKs (Fig. S2B and Table S5). Furthermore, two phospho-motifs, YXXXR and KXXXXY, were enriched during TGEV infection (Fig. S3B and Table S5), indicating that the most significantly phosphorylated amino acid during TGEV infection is tyrosine. The motifs identified above are found in many protein kinase and MAPK family substrates. In addition, TP is the only enriched threonine motif, and it is a substrate that commonly binds to the GSK-3, ERK1, ERK2, and CDK5 kinases (Fig. S3A and Table S5). The motif analysis along with the results of overrepresentation of phosphoproteins predicted to be substrates of MAPK support an increase in p38 and JNK1 activity during TGEV infection. A protein network related to TGEV/A9-regulated phosphoproteins was assembled by Ingenuity Pathway Analysis (IPA, versions 1.0 to 4.0), and 57 of the DRPs were recognized and mapped in the predicted network (Fig. S2C and Table S6). MAPK families, especially p38 (MAPK14) and JNK1 (MAPK8), were found to be important nodes that interact with many other proteins and were predicted to play important roles in the interaction network, and their phosphorylation levels were increased and then decreased during TGEV infection and subsequent A9 treatment mentioned above. This interaction network offers clues for further elucidation of the pathogenic mechanism of TGEV.

3.7. Validation of the differentially regulated phosphorylation of JNK1 and p38 by Western blotting analyses

To verify the DRPs identified in the phosphoproteomic analysis, we examined the lysates of TGEV-infected PK-15 cells by Western blotting with phospho-specific antibodies. In the TGEV-infected cells, the levels of p38 and JNK1 phosphorylation increased from 6 hpi to 36 hpi, while no change was detected in the total amount of p38 and JNK1 during the progression of TGEV infection. In uninfected cells, the phosphorylation statuses of p38 and JNK1 were weak and unchanged from 6 hpi to 36 hpi. In addition, the levels of total p38 and JNK1 proteins were consistent with those in TGEV-infected cells, at a relatively high level. Additionally, the phosphorylation status of p38 and JNK1 following TGEV infection was in accordance with the results of the phosphoproteomic analysis. The results showed that infection of PK-15 cells with TGEV activated p38 and JNK signaling, as evidenced by increased phosphorylation levels of p38 and JNK1 (Fig. 4A and B).

To investigate the relationships among A9, p38 and/or JNK1 and TGEV infection, we further assessed the phosphorylation and overall expression levels of p38 and JNK1 in TGEV-infected cells and in cells receiving A9 treatment by Western blotting. PK-15 cells were infected with TGEV at an MOI of 0.1 and treated with A9 or DMSO, and cell lysates were collected at 24 hpi for immunoblotting. As shown in Fig. 4C and D, phosphorylation of p38 and JNK1 was upregulated in TGEV-infected cells; DMSO treatment did not alter the upregulated p38 and JNK1 phosphorylation induced by TGEV infection. In contrast, the increase in p38 and JNK1 phosphorylation induced by TGEV infection was dramatically reduced by A9 treatment. The total protein levels of p38 and JNK1 were equivalent in the different treatment groups. Of these, we identified that p38 and JNK1 exhibited increased phosphorylation upon TGEV infection, and treatment of PK-15 cells with A9 resulted in downregulation of p38 and JNK1 phosphorylation in TGEV-infected cells. As above, we performed Western blotting to further measure the phosphorylation and overall expression levels of p38 in TGEV-infected cells (MOI of 1) and in cells receiving A9 treatment. As shown in Fig. 4E, A9 dramatically reduced the phosphorylation of p38 induced by TGEV infection.

3.8. The p38 inhibitor significantly decreases TGEV replication

To explore whether A9 affects TGEV replication by inhibiting downstream mediators of the p38 or JNK MAPK pathways, we treated TGEV-infected PK-15 cells with the specific inhibitor BIRB796 or DB07268 and determined the toxicity of inhibitors in PK-15 cells using the MTT assay. Concentrations of BIRB796 less than 80 μM and DB07268 less than 35 μM were not toxic to the tested cells (data not shown). PK-15 cells were also pretreated with different concentrations of inhibitors for 1 h prior to infection and then infected with TGEV at an MOI of 0.1, and virus titers were determined at 24 hpi by plaque assay. As shown in Fig. 5A, the p38 inhibitor reduced TGEV replication in a dose dependent manner compared with DMSO treated control cells. The inhibitory effects of the two inhibitors were significantly different, with marked inhibition observed for BIRB796 at 60 μM. In contrast, virus titers were only slightly reduced by treatment with DB07268, even at 30 μM, the concentration at which the maximal antiviral effect was observed without cytotoxicity. This finding suggests that DB07268 might not be as effective as BIRB796 at inhibiting TGEV propagation.

We further examined the kinetics of TGEV growth in PK-15 cells in the presence of an inhibitor or DMSO, and the results showed that the overall process of TGEV replication was markedly delayed when cells were treated with BIRB796 or DB07268 at their respective optimal concentration (Fig. 5B). Interestingly, we found that the amount of TGEV released into the medium was significantly reduced from 6 hpi to 24 hpi by treatment with BIRB796. In contrast, the virus yield was affected by DB07268 treatment between 12 hpi and 18 hpi, and the inhibitory effect of DB07268 on virus propagation was relatively weaker than that of BIRB796, suggesting that p38 activation plays a more important role in the viral life cycle than does JNK1.

We further examined the effects of BIRB796 and DB07268 on viral RNA synthesis and protein synthesis. TGEV-infected PK-15 cells were cultured in the presence of BIRB796, DB07268 or DMSO. The cells were collected at different time points post infection and the levels of the N gene were quantified. As shown in Fig. 5C, the mRNA abundance was approximately 10- to 20-fold lower from 6 to 24 hpi in cells treated with BIRB796 than in cells treated with DMSO alone, and the DB07268 treated group showed a reduction in TGEV N mRNA level by 2–5 fold. The results indicate that viral RNA synthesis was significantly inhibited by BIRB796 and DB07268. The amounts of viral structural protein N were also clearly reduced in both BIRB796-treated and DB07268-treated cells compared to that in DMSO-treated cells, with BIRB796 showing much greater effects, demonstrating that BIRB796 and DB07268 inhibited the synthesis of TGEV proteins (Fig. 5D). These results are in accordance with the N mRNA expression data. Together, these findings suggest that the p38 MAPK signaling pathway is required for efficient TGEV replication.

Finally, the essential regulatory role of p38 in TGEV infection was validated using a second p38-specific inhibitor, LY222820. We determined the toxicity of LY222820 in PK-15 cells using the MTT assay and found that LY222820 at a concentration less than 45 μM was not toxic to the tested cells (data not shown). TGEV-infected PK-15 cells were treated with the p38 inhibitor LY222820, and we determined the virus titers by plaque assay at 24 hpi. Overall, the data demonstrate that LY222820 significantly reduced TGEV replication (Fig. 5E). We also evaluated TGEV growth kinetics in PK-15 cells in the presence of LY222820, and the results were similar to the results reported above,

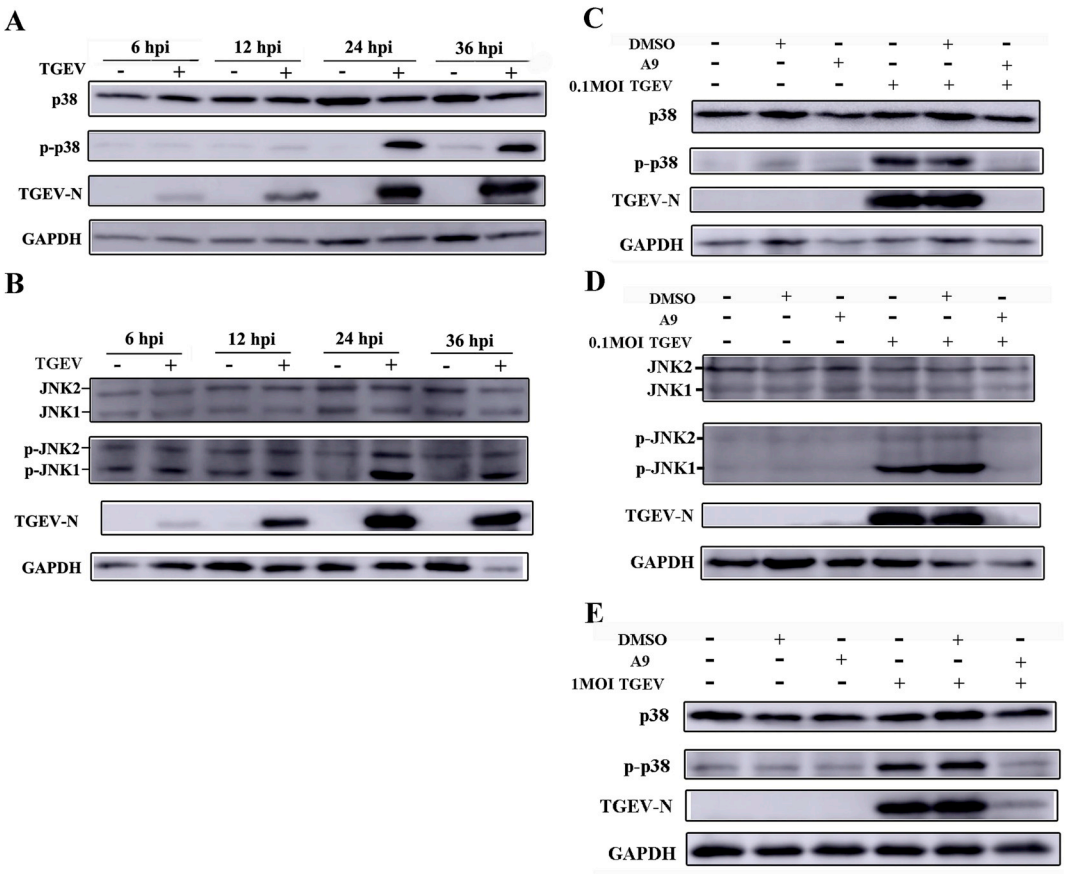

Fig. 4. The increased phosphorylation of p38 and JNK1 induced by TGEV infection is abolished by A9. (A) and (B) TGEV activates the p38 MAPK and JNK1/2 signaling pathways in cultured cells. Lysates from untreated control or TGEV-infected PK-15 cells at the indicated times were subjected to SDS-PAGE and immunoblotting using antibodies against phosphorylated p38, total p38, phosphorylated JNK, total JNK and the TGEV N protein. (C), (D) and (E) Activation of p38 and JNK1 is abolished by A9 treatment. PK-15 cells were treated with DMSO or A9, followed by TGEV infection or not at an MOI of 0.1 or 1. Untreated PK-15 cells were used as a mock control. Lysates of cells collected at 24 hpi were analyzed by immunoblotting using the indicated antibodies. GAPDH was detected to verify equal loading.

with the overall process of TGEV replication being markedly delayed when cells were treated with LY222820 (Fig. 5F).

3.9. The inhibitory activity of A9 against TGEV replication is mainly regulated by targeting p38

We used siRNA-mediated knockdown to further address whether A9 inhibits TGEV replication by targeting the downstream mediator p38. PK-15 cells were transiently transfected with siRNA targeting p38 or with negative control (NC) siRNA for 48 h, and the siRNA targeting p38 apparently reduced the expression of p38, as determined by Western blotting (Fig. 6A). Next, PK-15 cells in 12-well plates were transfected with p38 siRNA or NC siRNA for 48 h prior to infection with TGEV (MOI = 0.1), and the virus yield was determined by a plaque assay at different time points post infection. Compared to NC siRNA, the siRNA targeting p38 markedly decreased the viral titer by ~0.8 log (Fig. 6B) at 12 hpi. The specificities of A9 were also tested in NC siRNA transfected cells and p38-knockdown cells infected with TGEV. PK-15 cells were transfected with p38 siRNA or NC siRNA for 48 h and, then treated with 0.1 MOI TGEV and A9 for 12 h. Cells treated with TGEV and DMSO after transfection with siRNA were used as controls. The virus yield in supernatants at 12 hpi was detected by plaque assay. Interestingly, no difference in the inhibitory activity of A9 against TGEV was observed between p38-knockdown cells and NC siRNA-transfected cells (Fig. 6C). Collectively, the results indicate that p38 is a target through which A9 inhibits TGEV replication.

4. Discussion

LOPAC^{1280} is a collection of high quality, innovative drug-like molecules that have been used for a broad range of studies including cell signaling and neuroscience, and they reflect the most commonly screened targets in the drug discovery community. In this study, LOPAC^{1280} was used in the screening of anti-CoV drugs using TGEV as a surrogate model for CoV. Through successful HTS, a new antiviral drug candidate, A9, was identified and confirmed as the most prominent novel inhibitor of TGEV. In addition, A9 inhibited infectious PEDV, MHV and FIPV replication with similar potencies (Fig. 3). Kumar et al. have shown that A9 and AG879, two small-molecule RTKIs each potently block influenza virus replication at multiple steps of the viral life cycle and that the anti-influenza activity of AG879 may be due to its suppression of TrkA signaling, while the precise inhibitory mechanism of A9 remains unknown (Kumar et al., 2011a; Kumar et al., 2011b). The effects of A9 on TGEV replication and their underlying mechanisms in vitro were further explored in the present study.

4.1. The phosphorylation involved in the host response to TGEV infection is important for its replication

The effective replication of the virus depends on the host cell machinery. Similar to other viruses, CoV modulates several cellular pathways to enhance its replication by regulating the phosphorylation and dephosphorylation of host proteins, which is also the case for PEDV, SARS-CoV, MHV and MERS-CoV (Banerjee et al., 2002; Kim and Lee,

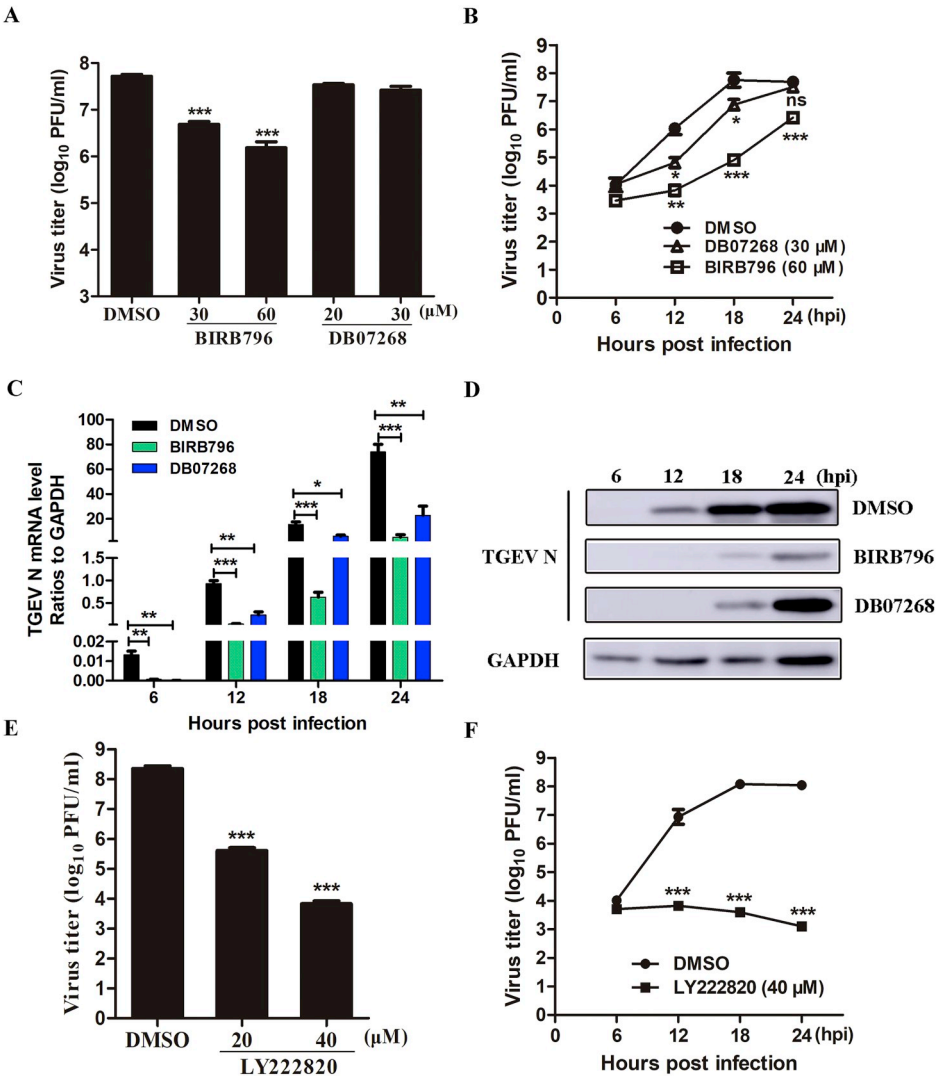

Fig. 5. TGEV propagation is suppressed by inhibition of p38 MAPK and JNK1/2 activation. (A and E) Effect of inhibitors on viral yields. PK-15 cells were pretreated for 1 h with the indicated inhibitor or DMSO, followed by TGEV infection at an MOI of 0.1 in the presence of an inhibitor. Virus titers in the supernatants of the cultures were measured at 24 hpi using PK-15 cells by plaque assay. (B and F) Effect of inhibitors on the growth curve of TGEV. PK-15 cells were treated with DMSO or inhibitor and infected at 0.1 MOI with TGEV. The cell culture supernatants were harvested at different time points as indicated. Virus titers were determined as described for panel A. (C) The inhibitor of p38 and JNK activation interferes with viral RNA synthesis. Inhibitor-treated or DMSO- treated PK-15 cells were infected with TGEV (MOI of 0.1) for 1 h and then cultivated in the presence of each inhibitor or DMSO. The viral RNA level was quantified at the indicated times by real-time RT-PCR and normalized to internal control pig GAPDH mRNA. (D) Chemical inhibition of p38 and JNK1 activation impairs viral protein synthesis. Western blot analysis of viral N protein at the indicated times in cells infected with TGEV (MOI of 0.1) and treated with DMSO or inhibitors. GAPDH detection was used to confirm equal loading. Each value is presented as the means of three independent experiments. Error bars indicate SD. Statistical analysis was conducted with Student's *t*-test (*$p < 0.05$, **$p < 0.01$, ***, $p < 0.001$).

2015; Kindrachuk et al., 2015; Lee et al., 2016; Mizutani et al., 2005). Nevertheless, no studies to date have focused on detecting global phosphorylation events in host cells during CoV infection. A9 is an RTKI and we hypothesized that its antiviral effect is most likely its influence on the phosphorylation of molecules downstream of RTKs in cells, which is required for viral replication. In this study, we applied quantitative phosphoproteome analysis to assess changes in cellular phosphoproteins involved in the host response to TGEV infection; 569 phosphoproteins from PK-15 cells and three viral proteins (matrix protein, spike glycoprotein and nucleoprotein) were identified (Table S1). Motif analysis suggested that the most significantly phosphorylated amino acid during TGEV infection is tyrosine (Fig. S3B), which is consistent with A9 acting as an inhibitor of RTK to inhibit the replication of TGEV. Several CoV N proteins have been shown to be phosphorylated and the phosphorylated sites for TGEV, avian infectious bronchitis virus (IBV) and MHV N proteins have been identified (Calvo et al., 2005; Chen et al., 2005; White et al., 2007). Chen and colleagues reported that phosphorylated IBV N protein presented a higher affinity for viral RNA than for nonviral RNA (Chen et al., 2005). Phosphorylation also plays an important role in the immunoreactivity and specificity of the SARS N protein (Shin et al., 2007). The phosphorylation status of the IBV N protein has the greatest impact on initiating the rescue of infectious virus from cDNA (Spencer et al., 2008). Phosphorylation modification is a unique strategy for CoV N to facilitate the synthesis of longer viral RNAs and subsequent viral progeny production, through the recruitment of cellular DDX1 (Wu et al., 2014). However, the function of the phosphorylated CoV N protein in viral pathogenesis is unknown, and further investigation is needed to determine whether the spike glycoprotein and matrix protein could be phosphorylated during CoV infection as well as the mechanism(s) by which coronaviral protein phosphorylation functions in viral replication. This study is the first to reveal global phosphorylation events in PK-15 cells induced by TGEV infection using quantitative phosphoproteomics and may therefore provide a basis for better understanding the molecular mechanisms of TGEV pathogenesis in addition to assisting in the development of antiviral drugs targeting TGEV.

4.2. p38 is one of the targets for the inhibitory activity of A9 against TGEV replication

Several studies have indicated that many downstream targets of RTKs are involved in CoV replication. Yang et al. found that PEDV infection stimulated the activation of EGFR and its downstream STAT3 cascade, which increased viral infection by negatively regulating type I interferon (IFN–I) signaling (Yang et al., 2018). The ERK/MAPK and PI3K/AKT/mTOR signaling responses play important roles in MERS-CoV infection (Kindrachuk et al., 2015), and JNK and phosphatidylinositol 3′-kinase (PI3K)/Akt are required for establishing persistent SARS-CoV infection in Vero E6 cells (Mizutani et al., 2005). Our phosphoproteomic analysis found that TGEV infection enhanced

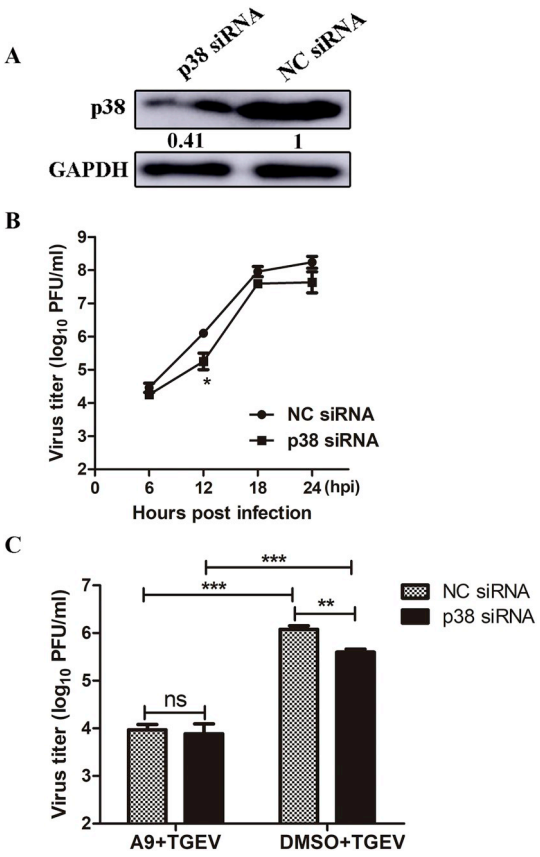

Fig. 6. p38 is one of the targets for the inhibitory activity of A9 against TGEV replication. (A) The efficiency of p38 siRNA was evaluated by Western blotting. PK-15 cells in 12-well plates were transfected with the indicated siRNA at 80 pmol using transfection reagent. At 48 h post transfection, the cells were lysed and subjected to Western blotting with an antibody against p38. Protein levels were quantified with ImageJ software and normalized to the amount of GAPDH. (B) Knock down of p38 expression with siRNA inhibited TGEV replication at 12 hpi. PK-15 cells in 12-well plates were transfected with p38 siRNA and NC siRNA at 80 pmol, respectively. At 48 h post transfection, the cells were infected with 0.1 MOI TGEV. Virus yield in supernatants of the cultures were measured at different time points using the plaque assay. (C) The effects of downregulating p38 MAPK on the inhibitory activity of A9 against TGEV replication. PK-15 cells were transfected with p38 siRNA or NC siRNA for 48 h, and then treated with 0.1 MOI TGEV and A9 for 12 h. Cells treated with TGEV and DMSO at 48 h post transfection were used as controls. Virus yield in the supernatants of the cultures was detected by plaque assay. The data shown are mean of three independent experiments (B and C). Statistical analyses used Student's *t*-test (*$p < 0.05$, **$p < 0.01$, ***$p < 0.001$).

phosphorylation of p38 and JNK1 by more than 10-fold and 3-fold, respectively, in TGEV-infected cells compared to that in untreated control cells (Fig. 4A and B, Fig. S1B and Table S2). In addition, p38 and JNK1 were not activated in PK-15 cells exposed to UV- inactivated TGEV (data not shown). These results indicate that activation of p38 and JNK MAPK is due to the actual replication of the virus in cells. However, tyrphostin A9 treatment can block TGEV-induced p38 and JNK1 phosphorylation (Fig. 4C and D and E and Table S2), indicating that p38 and JNK MAP kinase function downstream of RTKs. We further explored the effects of the downstream mediators of RTKs, p38 and JNK1, on TGEV replication using the specific inhibitors BIRB796 and DB07268, respectively. Our results showed that pretreatment with both BIRB796 and DB07268 significantly reduced TGEV N mRNA and protein levels (Fig. 5C and D), with a lower TGEV titer (Fig. 5A and B), compared to DMSO-treated control cells. We speculate that the inhibitory activity of A9 against TGEV replication might target multiple host kinases downstream of RTKs. RTKs are the primary mediators of many signals and control many downstream cascades, including phosphoinositide 3-kinase (PI3K), MAPK and $Ca2^+$ pathways (Schlessinger, 2000). Several studies have shown that phosphoinositide 3-kinase (PI3K) signaling and STAT3 cascades, which are downstream of RTKs, play important roles in the life cycle of CoV (Hu et al., 2016; Kindrachuk et al., 2015; Mizutani et al., 2005; Yang et al., 2018). Further studies are required to explore whether these downstream cascades are involved in the inhibitory activity of A9 against TGEV replication. To the extent that A9 might target multiple host components, drug-resistant viral variants are less likely to occur (Kumar et al., 2011a). Our results showed that the inhibitory effect of DB07268 on virus propagation was relatively weaker than that of BIRB796 (Fig. 5). Such a correlation suggests that A9 mainly inhibited the replication of TGEV through the p38 pathway. We also used another p38 inhibitor to validate its essential regulatory role in TGEV infection, and the results were consistent with those of BIRB796, which can significantly reduce TGEV replication (Fig. 5E and F). We also performed RNA interference to further validate that p38 plays an important regulatory role in TGEV replication (Fig. 6A and B). As the level of p38 expression was reduced to only 41% (Fig. 6A), residual p38 would still be phosphorylated during TGEV infection and promote virus replication. Moreover, other pathways also play a role in TGEV replication during A9 treatment, such as the JNK signaling pathway (Figs. 4 and 5). Therefore, the inhibitory effect of p38 siRNA was not as strong as the effect of the p38 inhibitor on viral replication. Furthermore, the specificities of A9 were tested in wild type and p38-knockdown cells with TGEV infection. Interestingly, the inhibitory activity of A9 against TGEV in p38-knockdown cells was similar to that of NC siRNA-transfected cells (Fig. 6C). All our results suggest that the inhibition of A9 on TGEV replication is mainly via targeting p38.

4.3. The possible mechanism by which p38 facilitates viral replication

MAPKs are important cellular signaling molecules that regulate cell growth, apoptosis, metabolism and differentiation under both normal and pathological conditions. The well characterized MAPKs are composed of three major groups: extracellular signal-regulated kinases 1 and 2 (ERK1/2, also known as p42/44 MAPK), p38 MAP kinases and JNKs (Schaeffer and Weber, 1999). The p38 MAPK pathway can be activated by a variety of CoVs and plays a crucial role in CoV infection. It has been reported that PEDV infection activates p38 MAPK and JNK1/2 and can exploit these molecules for optimal replication (Lee et al., 2016). Additionally, MHV infection activates p38 MAPK and JNK, which is necessary for its replication (Banerjee et al., 2002). Activation of p38 MAPK by FIPV regulates pro-inflammatory cytokine production which is a key contributor to the pathological changes observed in cats with FIP (Regan et al., 2009). p38 MAPK activation is required for human CoV 229E (HCoV-229E) replication and chloroquine inhibits HCoV-229E replication may by suppressing p38 activation (Kono et al., 2008). Our findings showed that A9 mainly inhibits TGEV replication through the p38 pathway. Moreover, A9 inhibited infectious PEDV, MHV and FIPV replication with similar potencies. Hence, it is reasonable to speculate that A9 may inhibit the replication of other CoVs by the same mechanism. Similar to other findings, tyrphostin A9 treatment inhibited gp120-induced p38 phosphorylation (Anand et al., 2009). Although the effect of p38 MAPK on viral replication has been studied in a variety of viruses, little is known about the mechanisms by which p38 activation facilitates virus replication. The author of one study discussed that stimulation of p38 MAPK may enhance the transcription of specific viral gene promoters, leading to the promotion of herpes simplex virus type 1 proliferation (Zachos et al., 2001). In MHV, p38 MAPK activation results in the phosphorylation of eIF4E, which facilitates virus protein synthesis and the subsequent production of infectious virus (Banerjee et al., 2002). Cencic et al. reported that targeting the eIF4F complex is a strategy for blocking CoV infection (Cencic et al., 2011). eIF4E is a downstream molecule of p38 MAPK and

increased eIF4E phosphorylation usually leads to enhanced translation rates (Gingras et al., 1999). Our results showed that TGEV-specific protein synthesis was decreased when infected cells were treated with BIRB796 (Fig. 5D). Therefore, whether viral replication is enhanced by p38 MAPK by modulating the downstream molecule eIF4E to increase viral protein synthesis in TGEV-infected cells remains to be determined.

TGEV infection induces high levels of p38 MAP kinase and JNK1 phosphorylation, both of which are required for TGEV replication. A9, an inhibitor of RTKs, initiates a signaling cascade that involves phosphorylation of the tyrosine kinase, in turn inhibiting the phosphorylation of p38 and JNK1, which are activated by TGEV infection; the result is a robust decrease in TGEV replication. In conclusion, although the signaling intermediates between TGEV and RTK remain to be elucidated, we identified and validated that p38 MAPK is a main downstream signaling node for the inhibitory activity of A9 against TGEV replication. The findings reported here provide novel insight into the molecular mechanisms underlying TGEV replication and offer new and promising therapeutic possibilities for combating infections caused by CoV. In summary, our findings show that TGEV infection can stimulate p38 and JNK1 phosphorylation and that A9 treatment can attenuate this phosphorylation status, which results in decreased TGEV replication. There has been significant progress in both clinical and preclinical studies of RTKIs as anti-cancer therapy in recent years, which may promote the development of such compounds for use in antiviral therapy.

Note

The mass spectrometry proteomics data have been deposited in ProteomeXchange Consortium via the PRIDE partner repository under the dataset identifier PXD010685.

Declaration of competing interest

The authors declare no conflict of interest.

Acknowledgements

This work was supported by the National Natural Science Foundation of China (Grant No. 31802207 and 31722056), the National Key R&D Plan of China (Program No. 2016YFD0500103 and 2018YFD0500100) and the Huazhong Agricultural University Scientific & Technological Self-Innovation Foundation (Program No. 2662015JQ003 and 2662017PY028).

Appendix A. Supplementary data

Supplementary data to this article can be found online at https://doi.org/10.1016/j.antiviral.2019.104651.

References

Anand, A.R., Prasad, A., Bradley, R.R., Deol, Y.S., Nagaraja, T., Ren, X., Terwilliger, E.F., Ganju, R.K., 2009. HIV-1 gp120-induced migration of dendritic cells is regulated by a novel kinase cascade involving Pyk2, p38 MAP kinase, and LSP1. Blood 114, 3588–3600.

Banerjee, S., Narayanan, K., Mizutani, T., Makino, S., 2002. Murine coronavirus replication-induced p38 mitogen-activated protein kinase activation promotes interleukin-6 production and virus replication in cultured cells. J. Virol. 76, 5937–5948.

Basu, A., Li, B., Mills, D.M., Panchal, R.G., Cardinale, S.C., Butler, M.M., Peet, N.P., Majgier-Baranowska, H., Williams, J.D., Patel, I., Moir, D.T., Bavari, S., Ray, R., Farzan, M.R., Rong, L., Bowlin, T.L., 2011. Identification of a small-molecule entry inhibitor for filoviruses. J. Virol. 85, 3106–3119.

Cai, Y., Liu, Y., Zhang, X., 2007. Suppression of coronavirus replication by inhibition of the MEK signaling pathway. J. Virol. 81, 446–456.

Calvo, E., Escors, D., Lopez, J.A., Gonzalez, J.M., Alvarez, A., Arza, E., Enjuanes, L., 2005. Phosphorylation and subcellular localization of transmissible gastroenteritis virus nucleocapsid protein in infected cells. J. Gen. Virol. 86, 2255–2267.

Carbone, C.J., Zheng, H., Bhattacharya, S., Lewis, J.R., Reiter, A.M., Henthorn, P., Zhang, Z.Y., Baker, D.P., Ukkiramapandian, R., Bence, K.K., Fuchs, S.Y., 2012. Protein tyrosine phosphatase 1B is a key regulator of IFNAR1 endocytosis and a target for antiviral therapies. In: Proceedings of the National Academy of Sciences of the United States of America, vol. 109. pp. 19226–19231.

Carstens, E.B., 2010. Ratification vote on taxonomic proposals to the international committee on taxonomy of viruses (2009). Arch. Virol. 155, 133–146.

Cencic, R., Desforges, M., Hall, D.R., Kozakov, D., Du, Y., Min, J., Dingledine, R., Fu, H., Vajda, S., Talbot, P.J., Pelletier, J., 2011. Blocking eIF4E-eIF4G interaction as a strategy to impair coronavirus replication. J. Virol. 85, 6381–6389.

Chen, H., Gill, A., Dove, B.K., Emmett, S.R., Kemp, C.F., Ritchie, M.A., Dee, M., Hiscox, J.A., 2005. Mass spectroscopic characterization of the coronavirus infectious bronchitis virus nucleoprotein and elucidation of the role of phosphorylation in RNA binding by using surface plasmon resonance. J. Virol. 79, 1164–1179.

de Groot, R.J., Baker, S.C., Baric, R., Enjuanes, L., Gorbalenya, A.E., Holmes, K.V., Perlman, S., Poon, L., Rottier, P.J.M., Talbot, P.J., Woo, P.C.Y., Ziebuhr, J., 2012. Virus taxonomy: ninth report of the international committee on taxonomy of viruses. In: King, A.M., Lefkowitz, E., Adams, M.J., Carstens, E.B. (Eds.), Family Coronaviridae. Elsevier Academic Press, San Diego, CA, pp. 806–828.

Dyall, J., Coleman, C.M., Hart, B.J., Venkataraman, T., Holbrook, M.R., Kindrachuk, J., Johnson, R.F., Olinger Jr., G.G., Jahrling, P.B., Laidlaw, M., Johansen, L.M., Lear-Rooney, C.M., Glass, P.J., Hensley, L.E., Frieman, M.B., 2014. Repurposing of clinically developed drugs for treatment of Middle East respiratory syndrome coronavirus infection. Antimicrob. Agents Chemother. 58, 4885–4893.

Falzarano, D., de Wit, E., Martellaro, C., Callison, J., Munster, V.J., Feldmann, H., 2013. Inhibition of novel beta coronavirus replication by a combination of interferon-alpha2b and ribavirin. Sci. Rep. 3, 1686.

Gan, F., Zhou, Y., Hou, L., Qian, G., Chen, X., Huang, K., 2017. Ochratoxin A induces nephrotoxicity and immunotoxicity through different MAPK signaling pathways in PK15 cells and porcine primary splenocytes. Chemosphere 182, 630–637.

Gingras, A.C., Raught, B., Sonenberg, N., 1999. eIF4 initiation factors: effectors of mRNA recruitment to ribosomes and regulators of translation. Annu. Rev. Biochem. 68, 913–963.

Gorbalenya, A.E., Enjuanes, L., Ziebuhr, J., Snijder, E.J., 2006. Nidovirales: evolving the largest RNA virus genome. Virus Res. 117, 17–37.

Hilgenfeld, R., Peiris, M., 2013. From SARS to MERS: 10 years of research on highly pathogenic human coronaviruses. Antivir. Res. 100, 286–295.

Hu, W., Zhu, L., Yang, X., Lin, J., Yang, Q., 2016. The epidermal growth factor receptor regulates cofilin activity and promotes transmissible gastroenteritis virus entry into intestinal epithelial cells. Oncotarget 7, 12206–12221.

Kim, Y., Lee, C., 2015. Extracellular signal-regulated kinase (ERK) activation is required for porcine epidemic diarrhea virus replication. Virology 484, 181–193.

Kindrachuk, J., Ork, B., Hart, B.J., Mazur, S., Holbrook, M.R., Frieman, M.B., Traynor, D., Johnson, R.F., Dyall, J., Kuhn, J.H., Olinger, G.G., Hensley, L.E., Jahrling, P.B., 2015. Antiviral potential of ERK/MAPK and PI3K/AKT/mTOR signaling modulation for Middle East respiratory syndrome coronavirus infection as identified by temporal kinome analysis. Antimicrob. Agents Chemother. 59, 1088–1099.

Kono, M., Tatsumi, K., Imai, A.M., Saito, K., Kuriyama, T., Shirasawa, H., 2008. Inhibition of human coronavirus 229E infection in human epithelial lung cells (L132) by chloroquine: involvement of p38 MAPK and ERK. Antivir. Res. 77, 150–152.

Kumar, N., Liang, Y., Parslow, T.G., Liang, Y., 2011a. Receptor tyrosine kinase inhibitors block multiple steps of influenza a virus replication. J. Virol. 85, 2818–2827.

Kumar, N., Sharma, N.R., Ly, H., Parslow, T.G., Liang, Y., 2011b. Receptor tyrosine kinase inhibitors that block replication of influenza a and other viruses. Antimicrob. Agents Chemother. 55, 5553–5559.

Lee, C., Kim, Y., Jeon, J.H., 2016. JNK and p38 mitogen-activated protein kinase pathways contribute to porcine epidemic diarrhea virus infection. Virus Res. 222, 1–12.

Lemmon, M.A., Schlessinger, J., 2010. Cell signaling by receptor tyrosine kinases. Cell 141, 1117–1134.

Meertens, L., Carnec, X., Lecoin, M.P., Ramdasi, R., Guivel-Benhassine, F., Lew, E., Lemke, G., Schwartz, O., Amara, A., 2012. The TIM and TAM families of phosphatidylserine receptors mediate dengue virus entry. Cell Host Microbe 12, 544–557.

Meertens, L., Labeau, A., Dejarnac, O., Cipriani, S., Sinigaglia, L., Bonnet-Madin, L., Le Charpentier, T., Hafirassou, M.L., Zamborlini, A., Cao-Lormeau, V.M., Coulpier, M., Misse, D., Jouvenet, N., Tabibiazar, R., Gressens, P., Schwartz, O., Amara, A., 2017. Axl mediates ZIKA virus entry in human glial cells and modulates innate immune responses. Cell Rep. 18, 324–333.

Mizutani, T., Fukushi, S., Saijo, M., Kurane, I., Morikawa, S., 2005. JNK and PI3k/Akt signaling pathways are required for establishing persistent SARS-CoV infection in Vero E6 cells. Biochim. Biophys. Acta 1741, 4–10.

Neuman, B.W., Chamberlain, P., Bowden, F., Joseph, J., 2014. Atlas of coronavirus replicase structure. Virus Res. 194, 49–66.

Pawson, T., 1995. Protein modules and signalling networks. Nature 373, 573–580.

Pritchard, G.C., Paton, D.J., Wibberley, G., Ibata, G., 1999. Transmissible gastroenteritis and porcine epidemic diarrhoea in Britain. Vet. Rec. 144, 616–618.

Ramajayam, R., Tan, K.P., Liu, H.G., Liang, P.H., 2010. Synthesis, docking studies, and evaluation of pyrimidines as inhibitors of SARS-CoV 3CL protease. Bioorg. Med. Chem. Lett 20, 3569–3572.

Regan, A.D., Cohen, R.D., Whittaker, G.R., 2009. Activation of p38 MAPK by feline infectious peritonitis virus regulates pro-inflammatory cytokine production in primary blood-derived feline mononuclear cells. Virology 384, 135–143.

Roussidis, A.E., Karamanos, N.K., 2002. Inhibition of receptor tyrosine kinase-based signal transduction as specific target for cancer treatment in vivo. vol. 16, 459–469 (Athens, Greece).

Schaeffer, H.J., Weber, M.J., 1999. Mitogen-activated protein kinases: specific messages from ubiquitous messengers. Mol. Cell. Biol. 19, 2435–2444.

Schlessinger, J., 2000. Cell signaling by receptor tyrosine kinases. Cell 103, 211–225.

Shin, G.C., Chung, Y.S., Kim, I.S., Cho, H.W., Kang, C., 2007. Antigenic characterization of

severe acute respiratory syndrome-coronavirus nucleocapsid protein expressed in insect cells: the effect of phosphorylation on immunoreactivity and specificity. Virus Res. 127, 71–80.
Spencer, K.A., Dee, M., Britton, P., Hiscox, J.A., 2008. Role of phosphorylation clusters in the biology of the coronavirus infectious bronchitis virus nucleocapsid protein. Virology 370, 373–381.
Stantchev, T.S., Markovic, I., Telford, W.G., Clouse, K.A., Broder, C.C., 2007. The tyrosine kinase inhibitor genistein blocks HIV-1 infection in primary human macrophages. Virus Res. 123, 178–189.
Tong, T.R., 2009. Drug targets in severe acute respiratory syndrome (SARS) virus and other coronavirus infections. Infect. Disord. - Drug Targets 9, 223–245.
Vela, E.M., Bowick, G.C., Herzog, N.K., Aronson, J.F., 2008. Genistein treatment of cells inhibits arenavirus infection. Antivir. Res. 77, 153–156.
White, T.C., Yi, Z., Hogue, B.G., 2007. Identification of mouse hepatitis coronavirus A59 nucleocapsid protein phosphorylation sites. Virus Res. 126, 139–148.
Wu, C.H., Chen, P.J., Yeh, S.H., 2014. Nucleocapsid phosphorylation and RNA helicase DDX1 recruitment enables coronavirus transition from discontinuous to continuous transcription. Cell Host Microbe 16, 462–472.
Yang, L., Xu, J., Guo, L., Guo, T., Zhang, L., Feng, L., Chen, H., Wang, Y., 2018. Porcine epidemic diarrhea virus-induced epidermal growth factor receptor activation impairs the antiviral activity of type I interferon. J. Virol. 92.
Yura, Y., Yoshida, H., Sato, M., 1993. Inhibition of herpes simplex virus replication by genistein, an inhibitor of protein-tyrosine kinase. Arch. Virol. 132, 451–461.
Zachos, G., Koffa, M., Preston, C.M., Clements, J.B., Conner, J., 2001. Herpes simplex virus type 1 blocks the apoptotic host cell defense mechanisms that target Bcl-2 and manipulates activation of p38 mitogen-activated protein kinase to improve viral replication. J. Virol. 75, 2710–2728.
Zhang, Y., Wei, Y., Li, J., Li, J., 2012. Development and optimization of a direct plaque assay for human and avian metapneumoviruses. J. Virol Methods 185, 61–68.
Zhou, Y., Agudelo, J., Lu, K., Goetz, D.H., Hansell, E., Chen, Y.T., Roush, W.R., McKerrow, J., Craik, C.S., Amberg, S.M., Simmons, G., 2011. Inhibitors of SARS-CoV entry–identification using an internally-controlled dual envelope pseudovirion assay. Antivir. Res. 92, 187–194.